

Electrochemical Determination of Ternatin in Ternate Grape Fern Herb Based on the Graphene-Au Nanocomposite

Xinyu Wang, Xinhua Fang, Hongnv Gan, Weier Jiang and Min Wu*

The Department of Pharmacy, Hangzhou Traditional Chinese Medicine Hospital, Hangzhou, 310000, P.R. China.

*E-mail: mingwu_hangzhou@yahoo.com

Received: 9 August 2016 / *Accepted:* 13 September 2016 / *Published:* 10 October 2016

A simple and effective electrochemical sensor with the electrode modified with RGO/Au (reduced graphene oxide-gold nanoparticle) nanocomposite was developed for the determination of ternatin. Microwave assisted approach was used for the preparation of RGO and then the RGO/Au was obtained by the electrodeposition of Au nanoparticles on RGO surface. Subsequently, electrochemical impedance spectroscopy (EIS) and cyclic voltammetry (CV) were employed for investigating the electrochemical performance of proposed sensor toward the reduction of ternatin. Obviously, the electrochemical activity of ternatin reduction was greatly improved with the employment of RGO/Au nanocomposite modified electrode. The linear response range from 2 μM to 600 μM was obtained on the sensor. In addition, the proposed sensor can be effectively applied to the detection of ternatin in grape fern herb as well.

Keywords: Electrochemical Sensor; RGO/Au/GCE; Ternatin; Grape fern herb

1. INTRODUCTION

As a group of naturally occurring polyphenolic substances that are widely distributed in plant kingdom, flavonoids are low molecular weight compound with pharmacological and biological activities [1]. Flavonoids are well known to have a positive effect on the various functional enzyme systems including phospholipases, cyclooxygenase, serine and threonine protein kinases, lipoxygenase and phospholipases that are critically involved in the initiation and maintenance of the inflammatory and immune response [2]. In addition, the lipid peroxidation inhibition and antioxidant properties can also be achieved by flavonoids [3-5]. What's more, the adhesion of molecules on endothelial-leukocyte was found to be inhibited by certain flavones or hydroxy-flavones [6].

As a kind of ferns, ternate Grape Fern Herb (also known as *Botrychium ternatum*) is seedless vascular plant. *Botrychium* species, a new species of moonworts, is an important kind of Chinese traditional medicine with multiple therapeutical functions such as heat-clearing, fire-purging, moisturising, detoxifying and anti-abortion as well. As the active component in *Botrychium ternatum*, ternatin is flavonoid compound that can be isolated from the crude drug and then used as therapeutical medicine. Besides, *Botrychium ternatum* is generally prepared as concentrated composite herbal preparations in oriental countries owing to the convenient usage. Therefore, to develop a simple, effective and economical technique for the determination of ternatin in Chinese traditional medicines is highly demanded. Unfortunately, the detection of ternatin is a completely unknown field till now with no research report.

Electrochemical technique, known as an effective analytical method, has various advantages including high accuracy and precision, good sensitivity and repeatability, large linear dynamic range and the requirement of relatively low-cost instrument as well [7-17]. In the field of medicine, a large number of pharmaceutical related problems can be effectively solved by electroanalytical methods. Recently, the electroanalytical method has been more widely employed for the component analysis of drugs in dosage forms or particularly biological samples as the development of more sensitive pulse methods.

Carbon based electrochemical sensors have acquired widespread use owing to their various advantages such as good biocompatibility, low cost, high chemical stability and good electron transfer kinetics. The traditional electrodes composed in carbon-based sensors were generally carbon fibers, glassy carbon and pyrolytic graphite. Recently, carbon nanomaterial has been a new-found electrode material that can be applied in the above-mentioned sensors with high performance. Normally, the size of nanomaterials is in the range of 1-100 nm, which results to high specific surface area and large surface-to-volume ratio. Therefore, carbon nanomaterials outperform many traditional electrode materials due to their enhanced electrocatalytic activity resulted from faster electron transfer kinetics and higher interfacial adsorption properties [18, 19].

In our work, ternatin was determined for the first time with a simple and accurate electrochemical sensor with graphene-Au nanocomposite modified electrode. With the constructed electrochemical sensor, the quality of ternatin of its pharmaceutical preparations circulating in the market can be effectively evaluated. In addition, the quality of ternatin during the medicinal manufacturing process can be effectively controlled.

2. EXPERIMENTAL

2.1. Chemicals

Ternatin (4',5-Dihydroxy-3,3',7,8-tetramethoxyflavone), $\text{HAuCl}_4 \cdot 3\text{H}_2\text{O}$, synthetic graphite (average particle diameter $<20 \mu\text{m}$) and PDDA (Poly(diallyl dimethyl ammonium chloride), 20 wt.%, $M_w=100000-200000 \text{ g/mol}$) were supplied by Sigma-Aldrich with further purification. Other chemicals are analytic reagents. Phosphate buffer solution (PBS) was synthesized as follows: firstly

mixing 0.1 M KH_2PO_4 solution and 0.1 M K_2HPO_4 solution together, and then the pH of mixed solution was adjusted. Milli-Q water (18.2 M Ω cm) was employed in the entire experiments.

2.2. Preparation of graphene-Au nanocomposite

Graphene oxide (GO) was synthesized according to the modified Hummers method [20, 21]. Reduced graphene oxide (RGO) was synthesized with a reported microwave heating method with certain variations [22]. Firstly, 5 mL of PDDA solution (1 mg mL⁻¹) was added into 5 mL of GO aqueous dispersion (0.5 g mL⁻¹), and then the obtained mixture was treated with sonication for 0.5 h. After adjusting the pH value to 12.0, the mixed solution was heated by microwave radiation for 5 min to generate the GO reduction and surface functionalization. Then the mixed solution was separated by centrifugation (10000 rpm, 10 min) and the obtained black sediment was rinsed with water three times. Lastly, the RGO (namely the obtained black sediment) was dried at 70°C in an oven for 12 h. The RGO/Au/GCE electrode was prepared by deposition of Au NPs and RGO on a GCE electrode with electrochemical method. Firstly, the GCE electrode was required to be polished with alumina-water slurry and then rinsed with ethanol and water. Then 5 μL of RGO dispersion (1 mg mL⁻¹) was dropped onto the clean GCE electrode. After the RGO/GCE electrode was completely dried at 25 °C, the Au NPs were deposited on the above-mentioned RGO/GCE electrode by electrochemical method. Chronoamperometry was carried out in the following conditions: RGO/GCE as working electrode, Ag/AgCl (3M KCl) as reference electrode and platinum wire as auxiliary electrode, 0.5 M H_2SO_4 solution containing 1% HAuCl_4 as electrolyte and -0.2 V as applied potential for 60s.

2.3. Characterization

The morphology of RGO/Au nanocomposite was measured with field emission scanning electron microscopy (FESEM, ZEISS SUPRA 55). The elemental information was collected from the EDX detector equipped on the FESEM. XRD patterns were observed on Bruker D8 Advance with Cu $\text{K}\alpha$ radiation ($\lambda = 0.1546$ nm) and the measured 2θ varied from 5° to 80°. UV-vis spectrophotometer (Perkin Elmer Lambda 950) and Raman Microprobe (Renishaw RM1000) was employed for optical analysis and Raman spectroscopy, respectively. Fourier transform infrared spectra (FTIR) were acquired from a Bruker Vertex 70 spectrometer.

2.4. Electrochemical determination

The CHI430A electrochemical working station with three electrode system (RGO/Au/GCE working electrode, Ag/AgCl reference electrode and Pt wire auxiliary electrode) was employed for the entire experiments. The resistance performance of RGO/Au/GCE electrode was characterized with electrochemical impedance spectroscopy (EIS). Specific experimental parameters were set as follows: 0.1 M KCl as electrolyte, 5 mM $[\text{Fe}(\text{CN})_6]^{3-/4-}$ as probe, 5 mV as amplitude and 10^1 - 10^5 Hz as frequency range. For the determination of ternetin, CV method was conducted in 0.1 M PBS with scan

range from -1.5 to -0.7 V at scan rate 50 mV/s. As to DPV measurement, the scan range was from -1.5 to -0.7 V with step potential of 0.6 mV/s and the modulation time was 0.05s with time interval of 0.2s.

2.5. Electrochemical determination of ternatin in grape fern herb

The purchased grape fern herb was firstly dried at 60 °C for 4 h, and then pulverized for usage. Subsequently, the pulverized powder (1 g) was refluxed with 70% aqueous ethanol (50 mL) for 1 h at 80°C. After the reflux was cooled down, a paper filter was used for the filtration. The mixture of extract and washings was concentrated to about 40 mL under vacuum. At last, this solution was diluted to 50 mL and used as real sample.

3. RESULT AND DISCUSSION

Raman spectroscopy was employed for confirming the formation of RGO by GO reduction because it is highly sensitivity to the electronic state change of carbon materials. As can be seen from the Raman spectra of GO and RGO/Au (Fig. 1A), the characteristic band at 1568 cm^{-1} corresponds to the graphite (G band, first-order scattering of E_{2g} phonons by sp^2 carbon atoms) and the other one at 1342 cm^{-1} is resulted from diamondoid (D band, breathing mode of κ -point photons of A_{1g} symmetry) [23]. In comparison with GO, RGO/Au nanocomposite possesses higher intensity ratio of D and G band (I_D/I_G), indicating that the average size of the sp^2 domains decreased and certain oxygen containing functional groups were removed as to RGO [24, 25].

The UV-vis spectra of GO, RGO and RGO/Au were shown in Fig. 1B. The absorption peak at 227 nm was resulted from $\pi-\pi^*$ transitions of C-C bonds for GO. Besides, a shoulder peak at 314 nm that can be assigned to $n-\pi^*$ transitions of C=O bonds was also observed [26]. As to the spectrum of RGO, only the absorption peak at 266 nm which probably caused by the red-shifts of the peak of GO at 227 nm was observed. Therefore, both the red shift phenomenon and disappearance of shoulder absorption peak indicated the successful reduction of GO to RGO. Moreover, the absorption peak at 545 nm resulted from the surface plasmon absorption of Au NPs was observed in the spectrum of RGO/Au composite, suggesting that Au NPs was successfully electrodeposited on RGO [27].

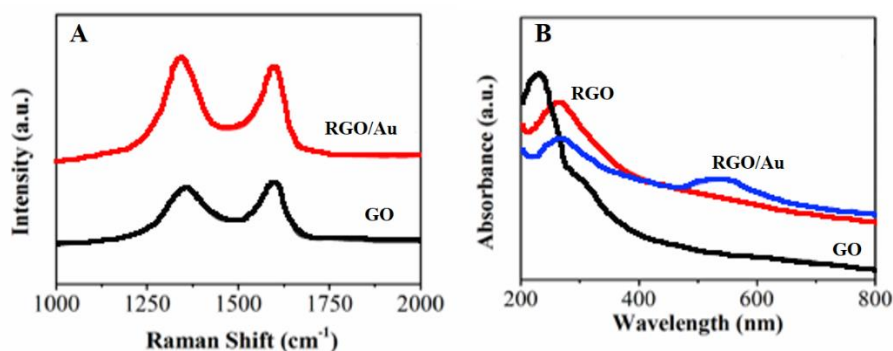


Figure 1. (A) Raman spectra of GO and RGO/Au. (B) UV-vis spectra of GO, RGO and RGO/Au nanocomposite.

The SEM images of RGO and RGO/Au nanocomposite were shown in Fig. 2A and Fig. 2B, respectively. The morphology of RGO was in the flake-like shape and wrinkled topology can be observed owing to the well dispersity of the RGO. As to RGO/Au nanocomposite, it was found that Au NPs were uniformly dispersed on RGO surface. The average size of dispersed Au NPs through calculating more than 100 samples was 60 nm. Fig. 2C showed the EDX characterization of RGO/Au nanocomposite. Only elements of Au, C and O could be observed, demonstrating the high purity composite.

Fig. 2D showed the XRD patterns of GO, RGO and RGO/Au nanocomposite. For GO, a characteristic peak at 11.0° was observed and it could be ascribed to the lattice plane (001) with d -spacing of 0.80 nm [28]. As to RGO, the peak at 2θ of 11.0° disappeared which indicated the completely reduction of GO. Besides, a broad peak at 2θ of 22.8° appeared which was resulted from the stacked graphene layers of RGO [29]. As to the XRD pattern of RGO/Au, the diffraction peaks at 38.3° , 43.6° , 63.5° and 76.9° correspond to the lattice plane (111), (200), (220) and (311) of Au NPs, respectively.

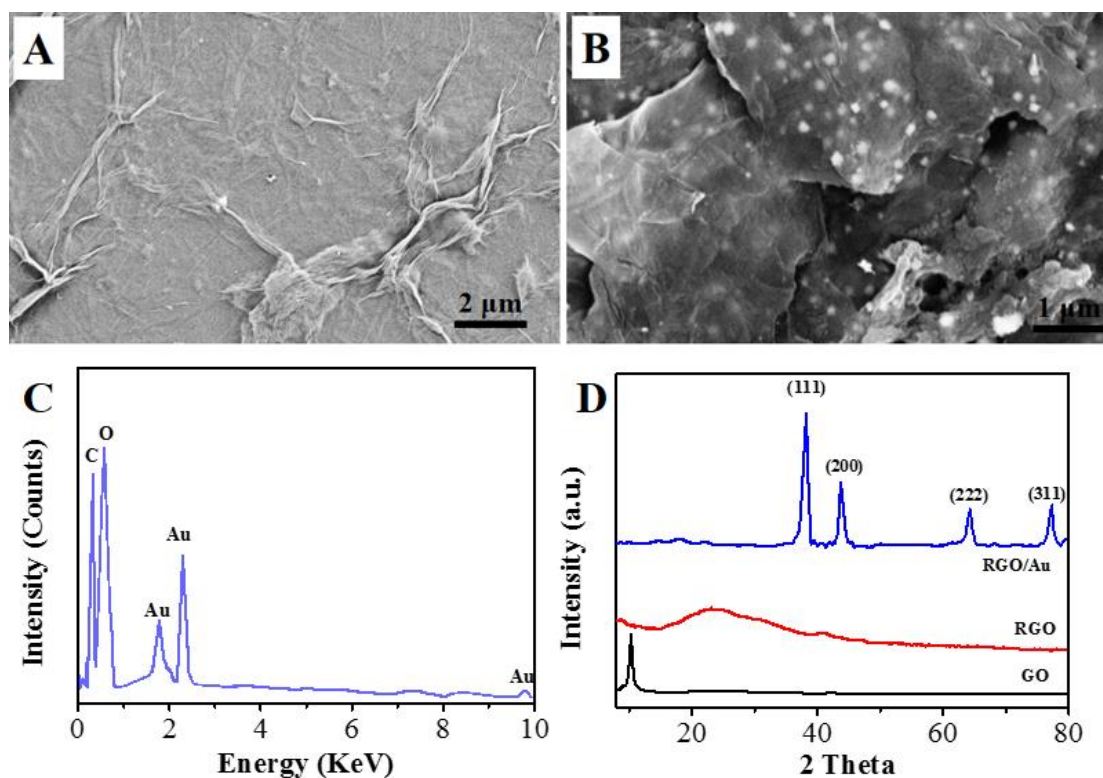


Figure 2. (A) SEM image of RGO, (B) SEM image and (C) EDX spectrum of RGO/Au composite, (D) XRD patterns of GO, RGO and RGO/Au.

Electrochemical impedance spectroscopy (EIS) was used to estimate the effects of modifications by RGO or RGO/Au on the electrochemical performance of GCE. Normally, EIS curve is composed of two parts including a semicircular (implication of the electron transfer process) and a straight line (implication of the diffusion process). Particularly, the electron transfer resistance value

can be obtained by calculating the diameter of semicircular. The measured EIS curves of bare GCE, RGO/GCE and RGO/Au/GCE toward 5 mM $[\text{Fe}(\text{CN})_6]^{3-/4-}$ solution was shown in Fig. 3. The diameter of semicircular obtained on RGO/GCE electrode was larger than that obtained on bare GCE electrode, indicating that the charge transfer was hindered after the immobilization of RGO on GCE electrode. The oxygen containing groups of RGO would limit the electron transfer of ferri/ferro cyanide, which resulted to more difficult charge transfer [30]. In contrast, the diameter of semicircular obtained on RGO/Au/GCE electrode was smaller than that obtained on bare GCE electrode, indicating lower electron transfer resistance of the redox-probe. Accordingly, the electrochemical performance of the electrode can be greatly improved by the addition of graphene sheets.

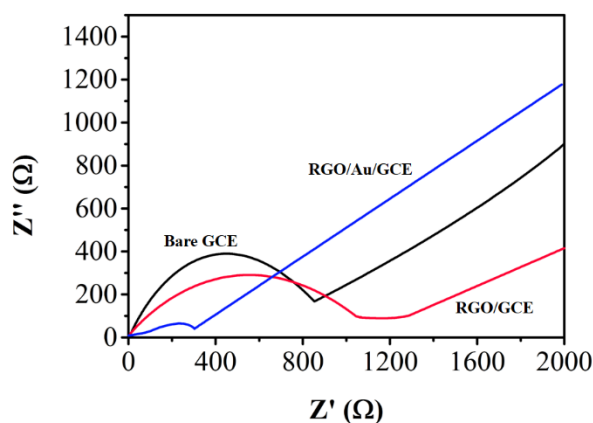


Figure 3. Nyquist diagrams obtained on bare GCE, RGO/GCE and RGO/Au/GCE electrodes.

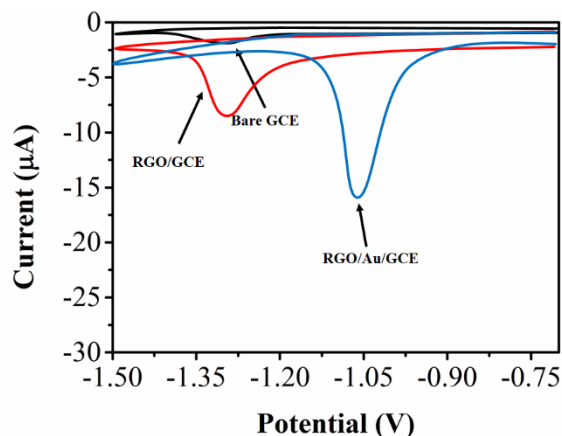


Figure 4. Cyclic voltammograms of 100 μM ternatin in PBS obtained on bare GCE, RGO/GCE and RGO/Au/GCE electrodes.

Cyclic voltammograms (CVs) of ternatin (100 μM) in PBS were conducted at different electrodes. As can be seen from Fig. 4, an irreversible response towards the reduction of ternatin was observed on all the three tested electrodes. Although higher electron transfer resistance was obtained on RGO/GCE electrode, the reduction response of ternatin obtained on RGO/GCE electrode was obviously higher than that obtained on bare GCE, which was ascribed to the enhanced adsorption of

ternatin molecules by larger specific surface area of RGO. In addition, the highest current response with the reduction potential positively shifted to -1.06 V was obtained on RGO/Au/GCE electrode. No peak could be observed without the addition of ternatin, which confirmed that the reduction peak appeared at -1.06 V was assured to be caused by the reduction of ternatin.

The effect of electrolyte on the performance of ternatin reduction was investigated. The reduction values measured in various electrolytes including 0.1 M PBS, $\text{Na}_2\text{C}_2\text{O}_4$, HAc-NaAc and H_2SO_4 were shown in Fig. 5A. Obviously, highest reduction response of ternatin was obtained with PBS as electrolyte. Thus, PBS was employed as the electrolyte in our study. The influence of pH value of PBS on the reduction performance of ternatin was also investigated and the results were given in in Fig. 5B. The peak current showed an increase with increasing pH value from 3 to 5, and then a decrease trend occurred with further increasing pH value. Consequently, pH value of 5 was the optimal value and used in our study. Fig. 5C showed the relationship between current response and the amount of Au NPs that depended upon electrodeposition time. The reduction current of ternatin was greatly improved with increasing electrodeposition time from 30 s to 60 s. When the deposition time was further increased to 90 s, a decline of the response was observed because the electrochemical reaction was hampered due to the aggregation of Au NPs.

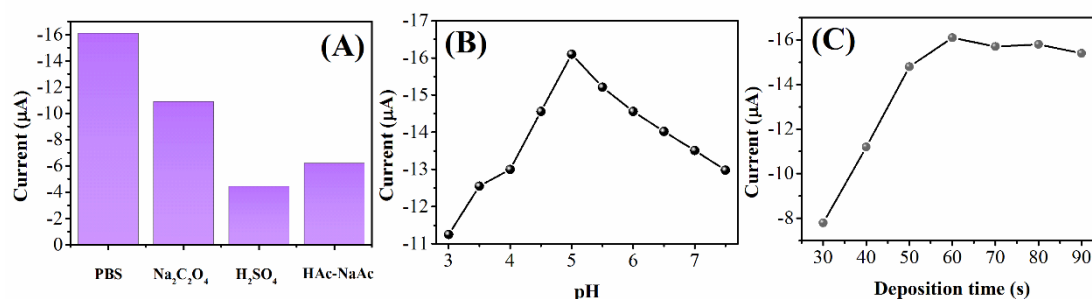


Figure 5. Effects of (A) electrolyte types, (B) pH values of PBS and (C) electrodeposition time on the reduction performance of ternatin.

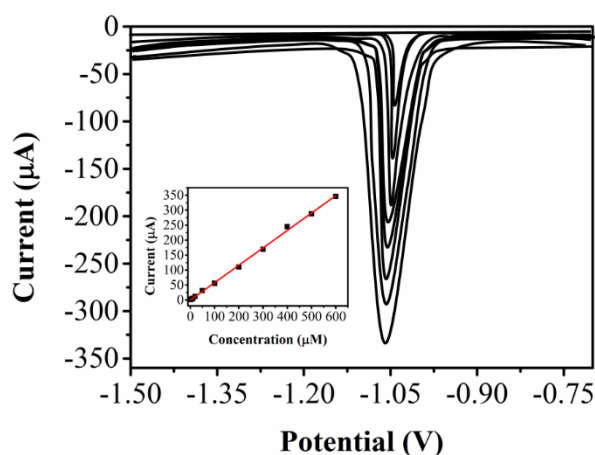


Figure 6. DPV curves of ternatin under various concentrations obtained on RGO/Au/GCE electrode. Inset: plot of reductive peak current in the function of ternatin concentration.

Differential pulse voltammetry (DPV) was employed to evaluate the analytical performance of RGO/u/GCE under obtained optimum conditions. DPV curves of ternatin under various concentrations

were obtained on RGO/Au/GCE electrode (Fig. 6). The current was related linearly with the concentration of ternatin varying from 2 to 600 μM , which was wider than previous report. As far as we know, the determination of ternatin by electrochemical technique was firstly reported. According to Yang et al. [31] report, different kinds of the aflatoxins can be used for inhibiting the detection of the ternatin. However, the aflatoxins such as avfA, omtA, and ver-1, coding for key enzymes in aflatoxin biosynthesis, showed no electrochemical response at the detection potential. Therefore, the proposed method has the potential for the detection of ternatin at the real conditions.

The reproducibility of the RGO/Au/GCE electrode was evaluated through the electrochemical reduction of 100 μM ternatin on ten fresh RGO/Au/GCE electrodes. The proposed electrochemical sensor for ternatin determination was confirmed to be excellently reproducible with the calculated relative standard deviation (RSD) being 3.15%. The stability of RGO/Au/GCE electrode toward the electrochemical reduction of 100 μM ternatin was evaluated by five identical tests. The current response was reduced by 3.77%. The current response of RGO/Au/GCE electrode was almost 96.4% of the initial value after stored in fridge for one month, demonstrating the long-term storage stability of RGO/Au/GCE.

The fabricated RGO/Au/GCE was also employed for the determination of ternatin in four grape fern herb extract samples. The validation was estimated with spike and recovery procedure. Table 1 showed the obtained results. Toward the detection of ternatin in four extract samples of grape fern herb, the achieved excellent performance suggested that our proposed electrochemical sensor with RGO/Au/GCE electrode is highly effective for the determination of ternatin in the real herb samples.

Table 1. Determination of ternatin in four grape fern herb extract samples with RGO/Au/GCE electrode.

| Sample | Addition (μM) | Found (μM) | Recovery (%) |
|--------|----------------------------|-------------------------|--------------|
| 1 | 0 | 17.27 | — |
| | 10 | 28.51 | 104.55 |
| 2 | 0 | 5.78 | — |
| | 50 | 56.21 | 100.77 |
| 3 | 0 | 8.96 | — |
| | 10 | 19.02 | 100.32 |
| 4 | 0 | 14.39 | — |
| | 50 | 64.11 | 99.57 |

4. CONCLUSION

In conclusion, a facial chemical method was used for the modification of GCE electrode with RGO. Subsequently, AuNPs was deposited on RGO by electrodeposition method. The as-prepared RGO/Au/GCE electrode was employed in the construction of electrochemical sensor for the

determination of ternatin. The linear response ranging from 2 to 600 μM was obtained on the proposed sensor. In addition, the good reproducibility and high stability was confirmed. The simple, reliable and sensitive electrochemical sensor for the determination of ternatin in the grape fern herb extract was reported for the first time.

References

1. P.C. Ferriola, V. Cody and E. Middleton, *Biochemical pharmacology*, 38 (1989) 1617
2. G. Di Carlo, N. Mascolo, A.A. Izzo and F. Capasso, *Life sciences*, 65 (1999) 337
3. M. Cholbi, M. Paya and M. Alcaraz, *Experientia*, 47 (1991) 195
4. A. Giaid and D. Saleh, *N. Engl. J. Med.*, 333 (1995) 214
5. A. Ubeda, M. Esteve, M. Alcaraz, K. Cheeseman and T. Slater, *Phytotherapy Research*, 9 (1995) 416
6. M.E. Gerritsen, W.W. Carley, G.E. Ranges, C.-P. Shen, S.A. Phan, G.F. Ligon and C.A. Perry, *The American journal of pathology*, 147 (1995) 278
7. S. Tajik, M.A. Taher, H. Beitollahi and M. Torkezadeh-Mahani, *Talanta*, 134 (2015) 60
8. Y.-L. Xie, J. Yuan, H.-L. Ye, P. Song and S.-Q. Hu, *Journal of Electroanalytical Chemistry*, 749 (2015) 26
9. P.T. Do, P.Q. Do, H.B. Nguyen, T.H. Le, L.H. Nguyen, H.V. Pham, T.L. Nguyen and Q.H. Tran, *Journal of Molecular Liquids*, 198 (2014) 307
10. G.F. Giordano, L.C.S. Vieira, A.L. Gobbi, R.S. Lima and L.T. Kubota, *Anal. Chim. Acta.*, 875 (2015) 33
11. V. Sharma, D. Hynek, L. Trnkova, D. Hemzal, M. Marik, R. Kizek and J. Hubalek, *Microchim. Acta.*, 183 (2016) 1299
12. A. Afkhami, T. Madrakian, M. Soltani-Shahrivar, M. Ahmadi and H. Ghaedi, *Journal of The Electrochemical Society*, 163 (2016) B68
13. X. Cao, H. Xu, S. Ding, Y. Ye, X. Ge and L. Yu, *Food chemistry*, 194 (2016) 1224
14. A.L. Santos, R.M. Takeuchi, R.A. Muñoz, L. Angnes and N.R. Stradiotto, *Electroanalysis*, 26 (2014) 233
15. X. Wang, X. Li and X. Tian, *Int. J. Electrochem. Sci.*, 10 (2015) 8361
16. L. Fu, Y. Zheng and A. Wang, *Int. J. Electrochem. Sci.*, 10 (2015) 3518
17. Y. Zheng, L. Fu, A. Wang and W. Cai, *Int. J. Electrochem. Sci.*, 10 (2015) 3530
18. S. Pérez, M. la Farré and D. Barceló, *TrAC Trends in Analytical Chemistry*, 28 (2009) 820
19. X. Yang, B. Feng, X. He, F. Li, Y. Ding and J. Fei, *Microchim. Acta.*, 180 (2013) 935
20. W.S. Hummers and R.E. Offeman, *Journal of the American Chemical Society*, 80 (1958) 1339
21. T. Gan and S. Hu, *Microchim. Acta.*, 175 (2011) 1
22. W. Liu, C. Li, Y. Gu, L. Tang, Z. Zhang and M. Yang, *Electroanalysis*, (2013) 2367
23. Z.-J. Fan, W. Kai, J. Yan, T. Wei, L.-J. Zhi, J. Feng, Y.-m. Ren, L.-P. Song and F. Wei, *ACS Nano*, 5 (2010) 191
24. X. Li, Q. Wang, Y. Zhao, W. Wu, J. Chen and H. Meng, *Journal of colloid and interface science*, 411 (2013) 69
25. S. Kamada, H. Nomoto, K. Fukuda, T. Fukawa, H. Shirai and M. Kimura, *Colloid Polym Sci*, 289 (2011) 925
26. J.I. Paredes, S. Villar-Rodil, A. Martínez-Alonso and J.M.D. Tascón, *Langmuir*, 24 (2008) 10560
27. X.C. Lv and J. Weng, *Scientific reports*, 3 (2013)
28. T. Nakajima, A. Mabuchi and R. Hagiwara, *Carbon*, 26 (1988) 357
29. D. Chen, L. Li and L. Guo, *Nanotechnology*, 22 (2011)
30. D.S. Jeykumari, S. Ramaprabhu and S.S. Narayanan, *Carbon*, 45 (2007) 1340

31. Z.-Y. Yang, W.-B. Shim, J.-H. Kim, S.-J. Park, S.-J. Kang, B.-S. Nam and D.-H. Chung, *Journal of Food Protection*®, 67 (2004) 2622

© 2016 The Authors. Published by ESG (www.electrochemsci.org). This article is an open access article distributed under the terms and conditions of the Creative Commons Attribution license (<http://creativecommons.org/licenses/by/4.0/>).